# A Microforce and Nanoforce Biomicroscope Device for *In Vitro* Mechanotransduction Investigation

Maxime Girot, Mehdi Boukallel, and Stéphane Régnier

***Abstract*—This paper deals with the development of an open design platform for explorative cell mechanotransduction investigation. The produced setup combines scanning probe microscopy (SPM) techniques and advanced robotics approaches, allowing both prolonged observations and spatial measurements on biological samples. As a result, an enhanced force probing method based on scanning microscopy techniques and advanced robotics and automation approaches is integrated in this device. Visual and force feedback control is used to achieve automatic data acquisition and monitoring processes when high skills are required. Experimentation on the mechanical cell characterization under *in vitro* conditions on human adherent cervix epithelial Hela cells are presented to demonstrate the viability and effectiveness of the proposed setup.**

***Index Terms*—Human adherent cervix epithelial Hela (EpH) cell mechanical characterization, *in vitro* mechanotransduction, scanning probe microscopy (SPM) techniques.**

## I. Introduction

MECHANOTRANSDUCTION is a cell process that converts mechanical stimuli into biochemical signals. Since most cells are sensitive to mechanical disturbances, the resulting response to mechanical inputs is a determinant in governing their behavior not only in the cell culture but in the whole organism as well. It is crucial to consider how external mechanical stimuli are transmitted into the cell. Many researches have been devoted to the understanding of the mechanotransduction mechanism. Despite these efforts, only a few studies lead to efficient models that predict force transduction to biochemical signals. Due to the complex cell behavior as well as the complex interactions involved in such a process, mechanotransduction is subjected to many assumptions. Despite this apparent complexity, it has, however, been shown that stimulated cells are activated by similar mechanisms at the molecular level.

Understanding the mechanotransduction basis first requires accurate knowledge of the magnitude and the distribution of forces sensed by the cell in their environment. Moreover, mechanical characterization of the cell properties is also required to correlate biological and mechanical behaviors. Actually, due to the structural complexity of cells (such as the deformable cytoskeleton formed by a 3-D intercellular network of interconnected biopolymers), detecting modifications in the mechanical properties of a cell can yield additional knowledge as to the way the cell reacts to mechanical stimuli.

Manuscript received April 16, 2007; revised March 12, 2008. First published May 30, 2008; current version published October 10, 2008.

The authors are with the Institut des Systèmes Intelligents et Robotique (ISIR), Université Pierre et Marie Curie-CNRS, 75005 Paris, France.

Color versions of one or more of the figures in this paper are available online at http://ieeexplore.ieee.org.

Digital Object Identifier 10.1109/TIM.2008.924928

The development of effective tools for mechanotransduction studies at the molecular level is crucial for understanding the involved mechanisms. The design of such tools should address important issues in terms of spatial and temporal features (e.g., measurements, positioning, and monitoring). In fact, due to the complexity of the cell mechanics, as well as the requirement of life science, suitable and specific solutions are needed. Robotics and microrobotics approaches can play an important role in the exploration of mechanotransduction mechanisms by the development toward highly effective and reliable systems.

## II. Motivations of This Work

A variety of approaches have been used to mechanically stimulate cells, sense force distribution, or determine cell mechanical properties [1]–[7]. Among these approaches, the most promising ones involve scanning probe microscopy (SPM) techniques for nanoscale. These techniques have the potential to give accurate quantitative information about local forces and contact mechanics. The atomic force microscope (AFM) has become a commonly used tool in the field of the biosciences [8]–[14]. A flexible cantilever with a low spring constant (0.1–0.2 N/m) and an atomic sharp tip is usually brought into the vicinity of the biological sample. The deflection of the cantilever, as a result of the mechanism interaction between the microindenter and the sample, is monitored by a split photodiode, and the use of a laser beam is reflected on the back of the cantilever. Some commercial solutions are available for the performance of experiments on life science (e.g., Veeco, Olympus, and Andor), but only a few of them are effective for mechanotransduction studies. The cost and the flexibility are the main drawbacks of these devices. Since these studies need complex experiments and specific environmental conditions, an open platform design is more suitable. Furthermore, studies on mechanotransduction are usually focused on a single cell target and are seldom conducted on a large cell population. Performing mechanotransduction on large samples, based on statistical approaches, can lead to better modeling at the molecular scale.

We associate some problems with the use of a standard commercial cantilever with a sharp tip for mechanotransduction requirements. In fact, the nanometer dimensions of the tip can cause important local strains that are higher than the elastic domain. Furthermore, depending on the magnitude of the force applied on the soft samples, both the cantilever tip and the samples can be easily damaged so that the local strain applied in the indented area becomes changed. Since mechanotransduction studies need accurate force application, a soft and noninvasive approach is more suitable. It must also

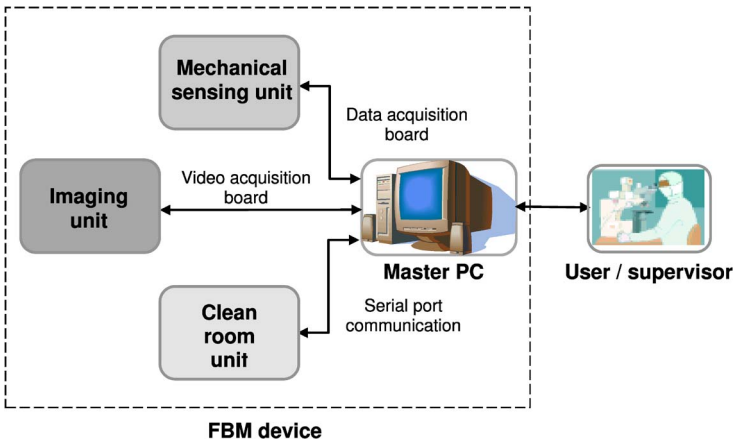


Fig. 1. Block diagram of the FBM device.

be emphasized that the force measured by the cantilever is calculated by a simple analytical formula (via Hooke's law) that expresses the force according to both the deflection and the spring constant of the lever. Consequently, the accuracy of the force-displacement data collected by the AFM is greatly dependent on the accurate knowledge of the spring constant since the deflection of the cantilever can be accurately detected by optical laser methods. Several authors have noted that the spring constants provided by cantilever manufacturers are incorrect [15], [16]. These significant errors are mainly due to the difficulty of accurately controlling their thickness during the microfabrication process. Much effort has been devoted to eliminating the necessity of knowing the cantilever thickness for the spring constant calibration process. As a result, various techniques have been developed and published, based on cantilever static or dynamic flexural deflection measurements [17]. The issue of the spring constant calibration using an accurate determination of the cantilever thickness is addressed in this paper. We use the dynamical frequency response method for thickness determination. As this method is quite accurate, the spring constant calibration is done according to the dimensions of the cantilever.

Another difficulty is associated with using sharp cantilevers. Usually, the spectroscopy curves collected with the AFM are used in conjunction with an appropriate analytical model to estimate Young's modulus, friction, wear, and other material properties. According to the literature, the Hertz model, which describes the relationship between force and indentation, is the commonly used approach for fitting the experimental data. In addition, two major assumptions are made: 1) linear elasticity and 2) infinite sample thickness. Some authors have shown that in the case of a soft contact mechanism, models derived from linear elasticity can lead to significant errors [12], [18]. Moreover, due to the imperfections of the tip radius of curvature, an unknown contact region results between the probe and the sample. Consequently, uncertainties are introduced to choose the appropriate fitting analytical model. It has also been shown that depending on the applied force and the sample's thickness, large errors may result when using infinite-thickness models [19], [20]. The authors compute force-displacement curves for finite sample thickness to show that for soft and thin samples, the error in the estimated elasticity modulus can be an order of magnitude. Costa and Yin [21] have also shown, using finite-element modeling, that linear-elasticity-derived models lead to significant errors in the case of sharp pyramidal tips.

In our opinion, mechanotransduction based on a tipless cantilever seems to be a promising solution. As studies involving such cantilevers are less prone to problems associated with a sharp-tip cantilever, enhanced nondestructive cell mechanical characterization should be achieved. For this purpose, a force biomicroscope (FBM) system has been developed that combines SPM techniques and advanced robotics approaches. A tipless chemically inert cantilever is used in this study. The spring constant calibration, using an accurate determination of the cantilever thickness, is addressed in this paper. We use a dynamical frequency response method for the spring constant cantilever calibration. Both cell mechanical properties and the contact mechanism are modeled with appropriate models, taking into account adhesion forces. More precisely, the Johnson, Kendall, and Roberts (JKR) and Derjaguin, Muller, and Toporov (DMT) contact theories are used to estimate both Young's modulus and the contact area that result from the mechanical characterization process. To demonstrate the accuracy of the JKR and DMT models in the case of soft contact mechanisms, the estimated force-deformation curves are compared with the one predicted by the Hertz theory.

## III. Experimental Setup Overview

The FBM device is a hybrid AFM that associates both the scanning microscopy approach and biological environment constraints. The FBM mainly consists of three units: 1) the mechanical sensing unit, which performs detection, positioning, and sensing features; 2) the imaging/grabbing unit for imaging and cell tracking features; and 3) the clean-room *in vitro* unit, which allows experiments to be conducted in a biological environment (Fig. 1). The overall configuration of the FBM and the different working components are shown in Fig. 2.

The FBM experimental setup provides suitable conditions for study in a controlled environment so that the biological cells can be kept in a living state for several hours by using a cage incubator. Therefore, the mechanical measurement process can be done on the biological sample over an extended period of time.

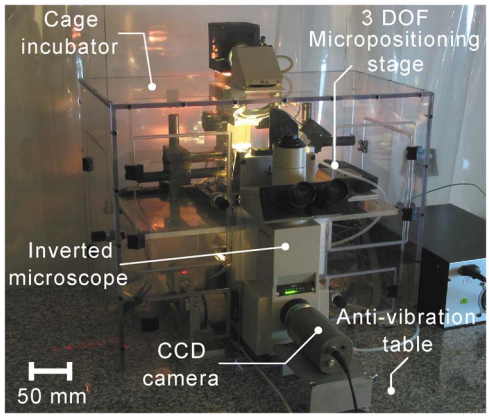


Fig. 2. FBM experimental setup overview.

A master computer is used to drive the FBM in an automatic operating mode based on force/vision referenced control. The data-acquisition process between the master computer and the FBM is achieved by the use of two specialized peripheral component interconnect cards (Matrox and National Instrument). A user-definable graphical interface has been developed to make the configuration of the experiments easier. To avoid undesired mechanical vibrations during the cell characterization process, the FBM experimental setup is installed on an antivibration table. The overall configuration of the FBM and the different working components are shown in Fig. 2.

### A. Mechanical Sensing Unit

The mechanical sensing unit is based on the detection of the deflection of a cantilever by an optical technique. A four-quadrant photodiode (CentroVision) with internal amplifiers associated with a 650-nm, low-power collimated laser diode (Vector Technology) is used to perform both axial and lateral nano-Newton force measurements. The total sensing area of the photodiode is 7 $mm^2$ with a spectral response from 400 to 1100 nm. The optical path of the Gaussian laser beam is optimized using a pair of mirrors and an aspheric condenser glass lens. Hence, the production of a sensitive and accurate detection device is the aim of our study. The sensitivity of the optical detection device is 5 $mV/\mu m$.

A low-spring-constant (0.2 N/m) uncoated tipless silicon cantilever (Nanosensors) is used as a probe for the cell mechanical characterization. The lever is 450 $\mu$m long, 90 $\mu$m wide, and 2 $\mu$m thick. The sample to be studied is accurately positioned below the cantilever by 3-degree-of-freedom ($x$-axial, $y$-lateral, and $z$-vertical) micropositioning encoded stages (Physik Instrumente) with a submicrometer resolution (0.1 $\mu$m). The kinematic features of the micropositioning stages allow us to achieve accurate mechanical measurements in a workspace of $25 \times 25 \times 25$ $mm^3$ with good repeatability. The configuration of the mechanical sensing unit, including the optical detection device, is presented in Figs. 3 and 4. A magnified picture of the cantilever with the focused laser beam on its reflective surface is shown in the same figure.

For the preliminary study, we focused on force feedback control of cantilever flexural deflection. Thus, only the vertical $z$ motion of a micropositioning stage is servoed. By knowing the vertical position of the micromotors as well as the deflection of the cantilever using the optical detection device, an optimized proportional and derivative (PD) controller was designed to ensure optimal control performance. The PD terms are optimized using the Ziegler–Nichols method. Fig. 5 shows experimental results on the force-referenced control approach for different desired forces.

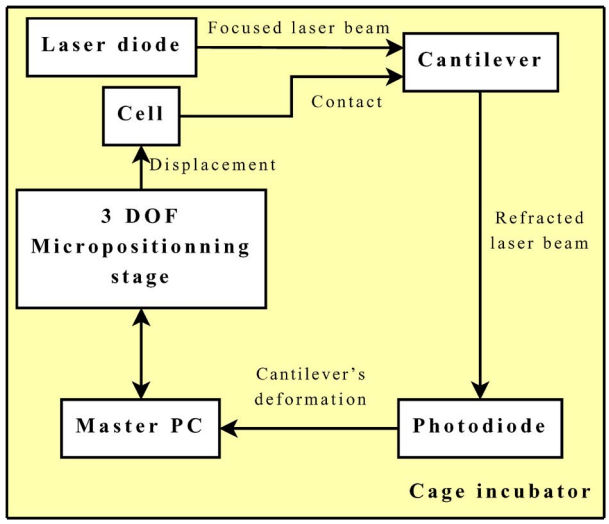


Fig. 3. FBM and mechanical sensing unit.

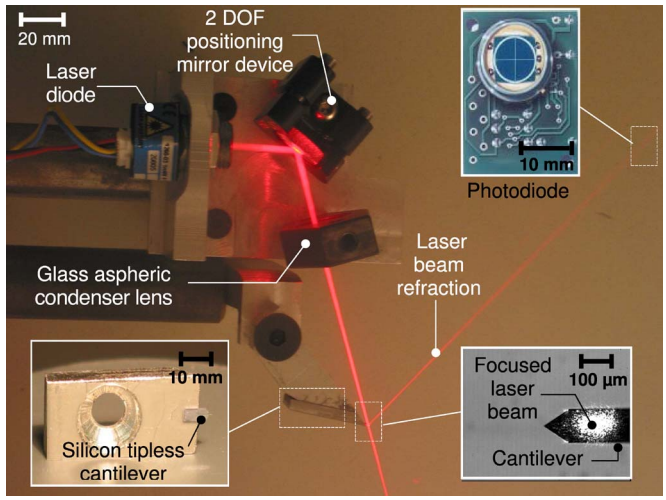


Fig. 4. Mechanical sensing unit.

### B. Imaging/Grabbing Unit

The imaging/grabbing unit consists of an inverted microscope (Olympus IMT-2) with Nikon 10× and 20× objectives. A phase contrast device is mounted on the microscope for precise contrast operation. The inverted microscope is fitted out with a charged-coupled-device (CCD) camera (754 × 488 pixel resolution). Using a frame grabber and a specialized imaging library package (Matrox Imaging) associated with the CCD camera, automatic mechanical characterization based on image feature tracking is achieved. The pixel-to-real-world

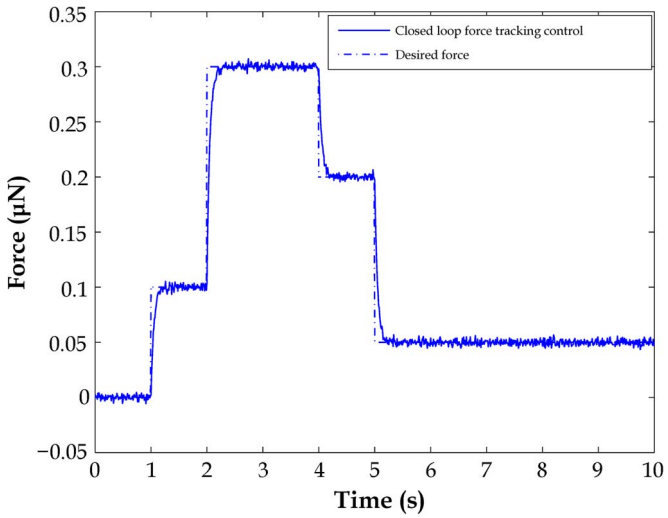


Fig. 5. Experimental results on the force feedback control approach.

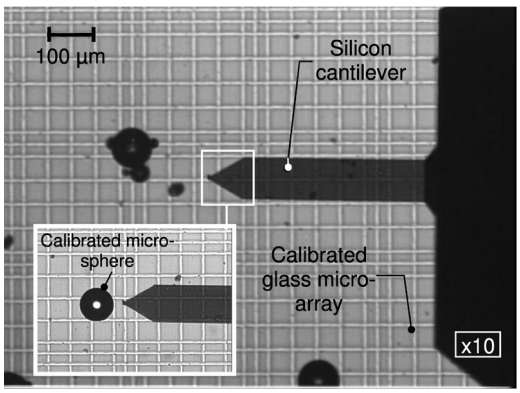


Fig. 6. Calibration of the CCD camera based on geometrical calibration.

calibration of the CCD camera is achieved by means of a calibrated glass microarray as well as calibrated microspheres (Fig. 6).

### C. Clean-Room Unit

The biological samples need specific requirements to be kept alive outside the *in vivo* conditions and to carry out prolonged observations. In addition to the biological nutrition medium, biological cells need a 37 °C temperature condition and 5% of $CO_2$ gas. The incubating system is formed by a controlled heating module that maintains temperature at 37 °C using a single thermocouple probe. The desired temperature of 37 °C is reached in 2 h. The cage incubator ensures a temperature stability within 0.1 °C. A mixed stream composed of 5% $CO_2$ and humidified air is fed into a small incubating chamber that contains the biological samples, thus avoiding condensation on the cage walls that could damage the mechanical parts of the microscope and the micropositioning stages. Temperature control is achieved by means of a configurable proportional-integral differential controller that communicates with a water bath via a serial port to the master computer. The whole system, including the FBM, is placed in a positive-pressure clean room to protect the biological environment.

TABLE I
SOLUTION OF (2)

| $\mu_1$ | $\mu_2$ | $\mu_3$ | $\mu_4$ |
|---|---|---|---|
| 1.875 | 4.693 | 7.854 | 10.995 |

## IV. CANTILEVER SPRING CONSTANT CALIBRATION

Since the beginning of scanning force microscopy, many methods for the spring constant calibration have been developed and studied. These methods agree to discard the use of the cantilever's dimensions since the determination of the thickness is problematic. To overcome this problem, we use a dynamical frequency response method for thickness determination. As this method is quite accurate, the spring constant calibration is done according to the dimensions of the cantilever.

The length and width of the cantilever are measured using an optical method by the same process used for camera calibration. The obtained values for length and width ($L = 450$ $\mu$m and $l = 90$ $\mu$m) are in good agreement with those of the manufacturer. Knowing all the dimensions of the cantilever, the spring constant is then calculated by a static method.

### A. Frequency Response Method for the Determination of the Cantilever's Thickness

Let us consider a cantilever of uniform section $S$, density $\rho$, Young's modulus $E'$, and inertial moment $I$. Each point of the cantilever should validate the classic wave equation for a beam in vibration, under the hypothesis of an undamped system

$$\rho S \frac{\partial^2 v}{\partial t^2} + E' I \frac{\partial^4 v}{\partial x^4} = 0 \tag{1}$$

where $v$ is the instantaneous deformation of the beam, depending on the time and position. The displacement can be written in two parts, i.e., one depending on the position along $x$-axis and another one on time: $v(x,t) = f(x)g(t)$.

To solve (1), i.e., to calculate the solution's constants, boundary conditions for the cantilever are needed. The fixed end of the cantilever must have zero displacement $(v(0) = 0)$ and zero rotation $(\theta(0) = 0)$. The free end of the cantilever cannot have a bending moment $(M(L) = 0)$ or a shearing force $(T(L) = 0)$.

The system of boundary equations accepts a solution only if the determinant is zero, which is equivalent to

$$1 + \cos\mu \cosh\mu = 0. \tag{2}$$

With $\mu = (\omega^2(\rho S/E'I))^{1/4}\alpha L$, (2) gives one condition on $\mu$ to be respected, which defines the eigenfrequency of the system. The first four solutions of this transcendent equation, which was numerically determined, are listed in Table I.

Given these solutions, if the length and the experimental eigenfrequency of the cantilever are known, the mean value of the thickness can easily be calculated by the following equation:

$$\langle h \rangle = \frac{1}{N} \sum_{i=1}^{N} \omega_i \frac{L^2}{\mu_i^2} \sqrt{\frac{12\rho}{E'}} \tag{3}$$

with $N$ being the number of the measured eigenfrequency.

TABLE II
ESTIMATED SPRING CONSTANT CANTILEVER

| | *Modes number* | | | |
|---|---|---|---|---|
| | 1 | 2 | 4 | |
| $\mu$ | 1.875 | 4.693 | 10.995 | theory |
| $f(kHz)$ | 12.63 | 82.4 | 446 | measured |
| $h(\mu m)$ | 1.516 | 1.579 | 1.557 | estimated |
| $k(N/m)$ | 0.187 | 0.211 | 0.202 | estimated |

In our case, the use of the eigenfrequency to determine the last dimension of the cantilever improves the accuracy, in comparison to the optical method, by a factor of 100. Moreover, this method can be achieved before each experimentation. Actually, the useful life of the cantilevers is very short (they can only be used once because of biological environment constraints), and the calibration process is repeated at every cantilever exchange.

### *B. Static Approach for the Spring Constant Cantilever Determination*

Knowing the dimensions of the cantilever and its material properties, the spring constant of a rectangular cantilever is given by $k = 3EI/L^3$, with the inertia momentum $I = lh^3/12$.

All the results for different modes (experimental results of mode 3 are unexploitable, because some mechanical parts of the microscope start resonating) are summarized in Table II.

The difference for the value of $k$ can be explained by the error on the measured eigenfrequency but also because the estimated thickness is a mean value. Actually, the variation of the thickness all along the cantilever affects the eigenfrequency of each mode differently.

The variation from the mean value of $k$ is small and acceptable, and the logarithmic error is about 3.7%, with a contribution of the thickness for this error of 1.9%. In comparison with the spring constant announced by the manufacturer, the mean value is close for this batch, but the uncertainty is lower (3.7% instead of 90%).

### *C. Experimental Spring Constant Cantilever Validation*

These experiments aim to validate the force measurement accuracy of the mechanical sensing unit, including the cantilever and the optical laser system. Two measurements are performed. In the first one, a previously calibrated cantilever is pressed onto a rigid substrate. For the second one, another calibrated cantilever (from the same batch) is pressed against the other one. A silicon sphere is placed between the two cantilevers to avoid adhesion effects and to guarantee punctual contacts on both sides (Fig. 7).

The cantilever/substrate mechanical interaction is used to calibrate the whole system. The photodiode gives an output voltage that corresponds to the translation (tilt) of the laser beam. As the cantilever has been calibrated before, for a displacement of 1 $\mu$m, the sensed force is 0.2 $\mu$N. This technique allows us to calculate the laser optical path as well as the accurate calibration of the photodiode. In the case of cantilever/cantilever interaction, the mechanical system is considered to be two springs in series, with respective spring constants $k_1$ and $k_2$. The equivalent stiffness $K_{eq}$ can be expressed as a function of $k_1$ and $k_2$ as follows: $1/K_{eq} = 1/k_1 + 1/k_2$. Fig. 8 shows the experimental force sensed by the measuring cantilever for both the rigid subtract and the cantilever/cantilever mechanical interaction. Since the spring constant corresponds to the gradient of curves, the cantilever/cantilever curve leads to a value of $K_{eq} = 0.101$ N/m on average. As the measuring cantilever is calibrated ($k_1 = 0.201$ N/m), we found that $k_2 = 0.203$ N/m, which is in accordance with the expected results.

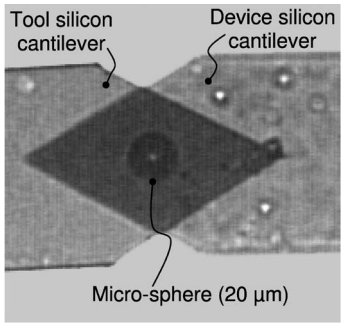


Fig. 7. Cantilever/sphere/cantilever contact.

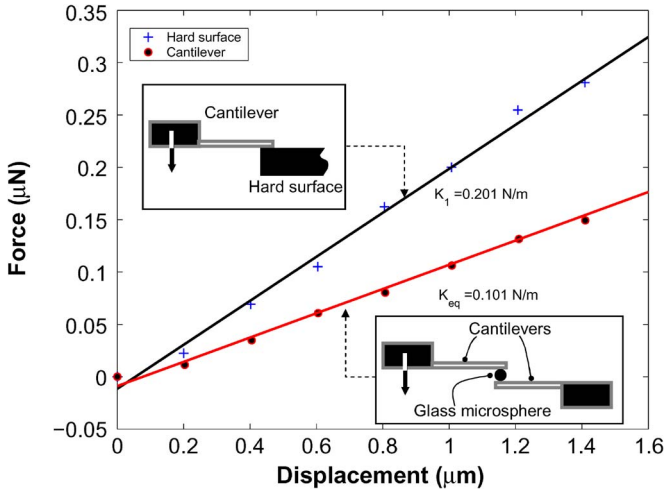


Fig. 8. Experimental determination of the cantilever spring constant.

## V. *IN VITRO* MECHANICAL CHARACTERIZATION EXPERIMENTS

The epithelial Hela *(EpH)* cells are prepared on petri dishes with a specific culture medium formed by Dulbecco's modified eagle's medium with high glucose and L-glutamine components and 10% of fetal bovine serum (Fig. 9). The cervix *(EpH)* cells can be morphologically assimilated to an elliptical cell with a thin surrounding biomembrane, which has two functions: 1) ensuring the protection of the cytoplasm and 2) ensuring the adhesion feature on the substrate. In this paper, the average dimensions of the biological sample are 10 $\mu$m long, 9 $\mu$m wide, and 6 $\mu$m in height.

### *A. Cell's Mechanical Response Characterization*

Fig. 10(a) shows the experimental curves of the photodiode output as a function of the sample vertical displacement ($\Delta z$)

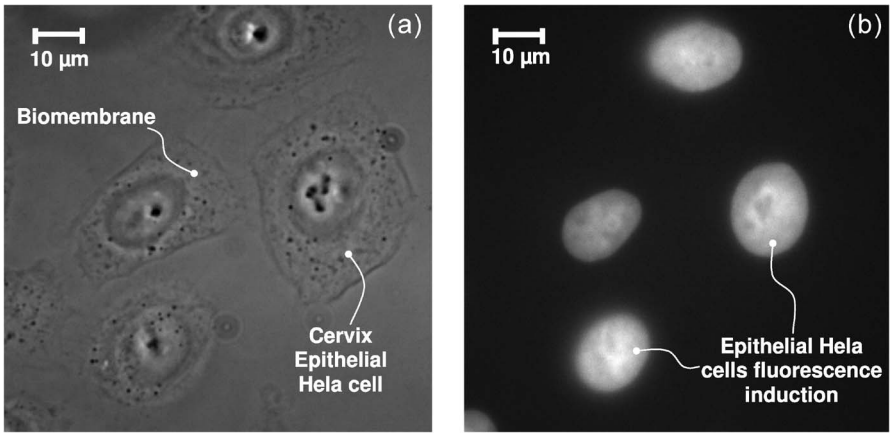


Fig. 9. (a) Magnified image of the cervix *EpH* cells obtained with a 63× objective. (b) Cervix *EpH* cells morphology observed by fluorescence techniques.

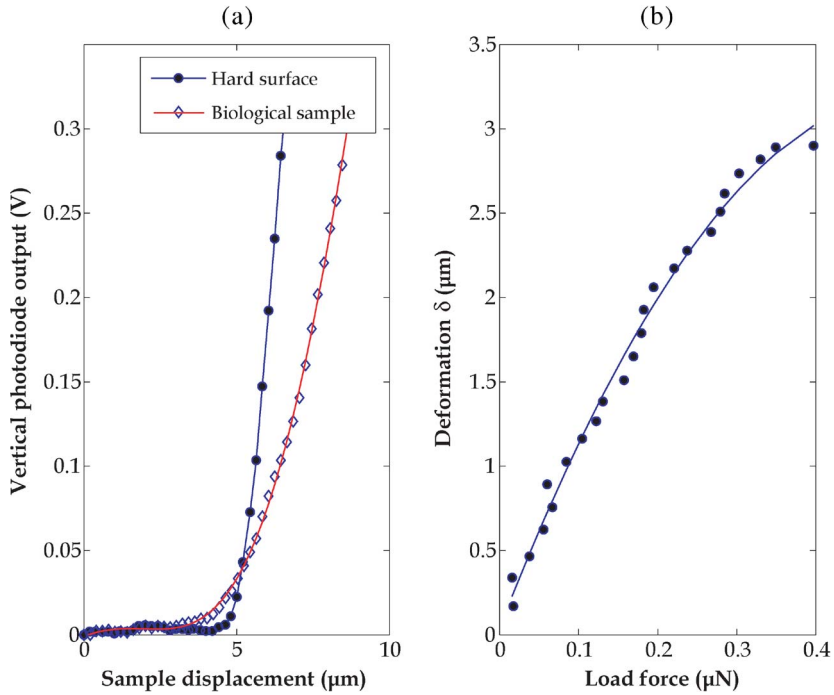


Fig. 10. (a) Experimental data of the photodiode output as a function of the sample displacement performed on both a single *EpH* cell and a hard surface. (b) Experimental curve of the sample deformation $\delta$ as a function of the applied load by the cantilever.

performed on both a single *EpH* cell and a hard surface. The single step of the sample displacement is 200 nm, and the total displacement is 8 $\mu$m. The deformation $\delta$ of the *EpH* cell is monitored by calculating the difference between the sample displacement $\Delta z$ and the cantilever deflection $\Delta d$. The nonlinear elastic behavior of the *EpH* can be seen in Fig. 10(b), which presents the sample deformation $\delta$ as a function of the load force applied by the cantilever.

The viscoelastic behavior of the *EpH* cells are also investigated by the FBM device. A cyclical automatic approach and retract experimentations were conducted on the same biological sample for 2 h at 3-min intervals. In this paper, the motion amplitude and the single step of the vertical microstage are fixed to 8 $\mu$m and 200 nm, respectively. To reduce the cantilever damping oscillations during the mechanical characterization process, the velocity of the sample positioning stage is chosen to be small (0.5 $\mu$m/s). Fig. 11(a) shows three approach and retract curves monitored at different time intervals ($t = 0$, 40, and 80 min) of the cyclical experiments. A single referenced approach and retract curves performed on a hard surface are given in Fig. 11(b). According to the collected data, the *EpH* sample exhibits the same viscoelastic behavior during all experimentations.

### *B. In Vitro Efficiency Approach for Cell Mechanical Characterization*

To address either the efficiency of the *in vitro* clean-room unit or how mechanical cell properties can be affected by the environmental culture conditions, we have experimented with automatic and cyclical spectroscopy operation on a single *EpH* cell for several minutes without the use of the incubating system. As the precedent study, the sample displacement and the single step of the vertical micropositioning stage are

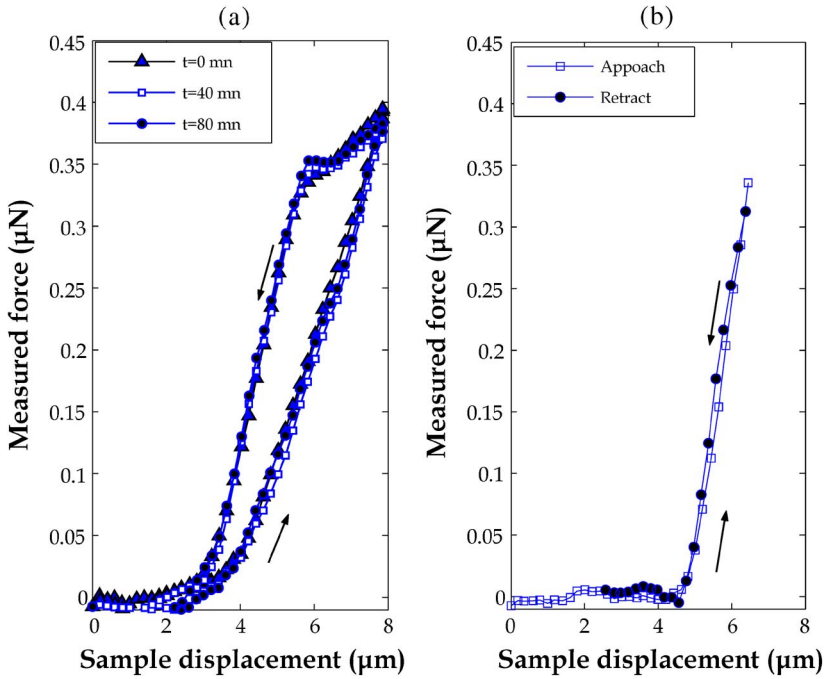


Fig. 11. (a) Experimental spectroscopy curves (approach and retract) performed on a single *EpH* cell at different time intervals ($t = 0$, 40, and 80 min). (b) Single referenced approach and retract curves performed on a hard surface.

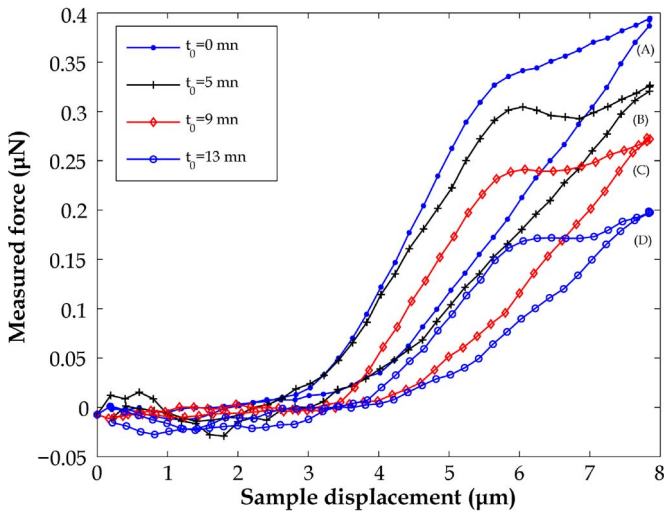


Fig. 12. Evolution of the measured force as a function of the sample displacement for different elapsed times $t_0 = 0$, 5, 9, and 13 min.

fixed to 8 $\mu$m and 200 nm, respectively. Since the purpose of this study is to observe the difference that can occur on the mechanical behavior of the studied biological sample, experimentation is initially conducted using the incubating system. Fig. 12 shows the evolution of the *EpH* cell mechanical behavior of cyclical spectroscopy operation with and without the use of the incubating system. More specifically, curve (A) shows the approach and retract curves using the cage incubator. Curves (B)–(D) show the mechanical behavior of the studied *EpH* cell for different elapsed times $t_0$ once the cage incubator is turned off.

These mechanical characterization experiments obviously reveal that the mechanical properties of the studied sample are affected by the temperature environmental culture conditions.

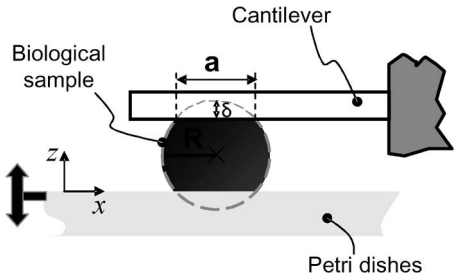


Fig. 13. Mechanical interaction scheme between the silicon tipless cantilever and the biological sample.

This difference suggests that the intracellular or extracellular matrix react to the variation of temperature.

### C. Analytical Model for Both Young's Modulus and Contact Area Estimation

Young's modulus $E$ and the contact area $a$ that result from the *EpH* cell mechanical characterization process are estimated using an appropriate analytical fitted model. Since Young's modulus can be used to predict the elongation or compression of the biological sample as long as the stress is less than the yield strength of the sample, the chosen models are fitted to sample deformations where elastic linear properties are satisfied. According to curve (B), the quasi-linear elastic behavior is satisfied for load $P$ less than 0.15 $\mu$N. Three analytical models are chosen to estimate Young's modulus and the contact area. Thus, the Hertz, JKR, and DMT models, respectively, are used.

Fig. 13 presents the mechanical interaction between the silicon tipless cantilever and the biological sample. Noting the radius of the biological sample $R$ ($R = 5$ $\mu$m), the adhesion work $w$, and the load force applied by the cantilever $P$, the

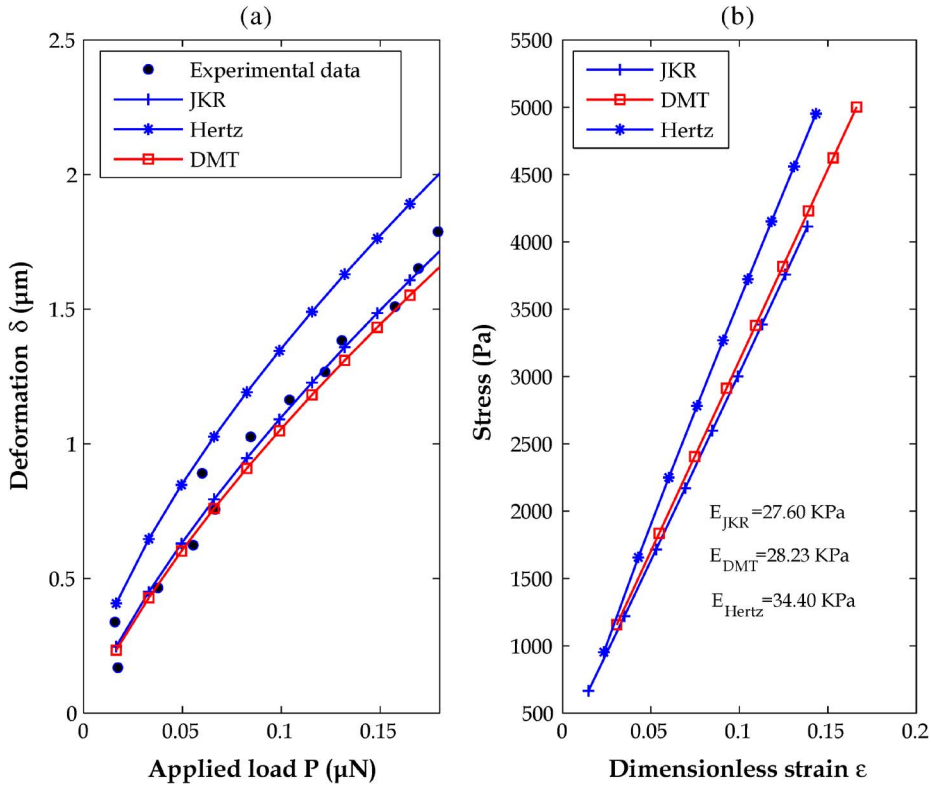


Fig. 14. (a) Estimation of the biological sample deformation $\delta$ as a function of the simulated load force $P$ using the Hertz, JKR, and DMT theories compared to the experimental data. (b) Estimated stress $\sigma = P/a$ as a function of the estimated strain $\varepsilon = \delta/2R$ using the Hertz, JKR, and DMT theories.

contact area $a$ can be expressed, respectively, according to the Hertz, JKR, and DMT theories [22]

$$a^3 = \frac{RP}{K} \tag{4}$$

$$a^3 = \frac{R}{K}\left(P + 3\pi Rw + \sqrt{6\pi RwP + (3\pi Rw)^2}\right) \tag{5}$$

$$a^3 = \frac{R}{K}(P + 2\pi Rw) \tag{6}$$

where $K$ is the effective Young's modulus of the two materials in contact. $K$ is expressed according to the Hertz, the JKR, or the DMT model as

$$\frac{1}{K} = \frac{3}{4}\left(\frac{1-\nu^2}{E} + \frac{1-\nu'^2}{E'}\right) \tag{7}$$

where $\nu$ and $\nu'$ are, respectively, the Poisson's coefficients of the *EpH* cells ($\nu = 0.5$) and the silicon cantilever. The manufacturer's data give Young's modulus of the silicon tipless cantilever and Poisson's ratio as $E' = 140$ GPa and $\nu' = 0.17$.

The JKR and DMT theories suggest that adhesion work $w$ can be expressed in two ways according to the pull-off force $P_{\text{off}}$ needed to overcome adhesion forces as [22]

$$P_{\text{off}} = \frac{3}{2}\pi Rw(\text{JKR}) \tag{8}$$

$$P_{\text{off}} = 2\pi Rw(\text{DMT}). \tag{9}$$

As the pull-off force $P_{\text{off}}$ is accurately measured using the FBM ($P_{\text{off}} \simeq 20$ nN), the adhesion work $w$ is introduced in (5) and (6) to estimate the contact area $a$.

The deformation $\delta$ of the elastic body is expressed, respectively, using the Hertz, JKR, and DMT analytical models as [22]

$$\delta_{\text{Hertz}} = \delta_{\text{DMT}} = \frac{a^2}{R} \tag{10}$$

$$\delta_{\text{JKR}} = \frac{a^2}{R} - \sqrt{\frac{8\pi wa}{3K}}. \tag{11}$$

Fig. 14(a) shows the estimation of the biological sample deformation $\delta$ as a function of the simulated load force $P$ using the Hertz, JKR, and DMT theories. These analytical results are compared to the experimental measurements performed with the FBM and presented in Section V-A. The *EpH* cells' Young's modulus $E$ is estimated using the biological sample deformation $\delta$ and the contact area $a$ obtained by the different modeling approaches. Fig. 14(b) shows the estimated stress $\sigma = P/a$ as a function of the estimated strain $\varepsilon = \delta/2R$ using the Hertz, JKR, and DMT theories. Since linear elastic deformation is satisfied, Young's modulus $E$ of the studied biological sample can be determined by calculating the slope of the obtained curves ($\sigma = E\varepsilon$). These results emphasize, in our case, that the Hertz model is not appropriate for the estimation of the contact mechanism in the case of soft materials at the microscale. Since adhesion forces are not considered, large errors are observed between the experimental data and the predicted force-deformation curves (on the order of 0.2 $\mu$m of magnitude). We have observed a small deviation between the JKR and the DMT models to estimate the force-deformation curve. According to [22], the DMT theory is applied in the case of hard solids, with a small radius of curvature and low energy of adhesion. The JKR

theory is more often applied for soft solids, with a large radius and large energy of adhesion. Based on these considerations, we chose the JKR model as the model reference in our case. This model, used in conjunction with the experimental data, leads to an accurate detection of cell mechanical property modification needed in mechanotransduction studies.

### D. Parametric Models' Accuracy Evaluation

Errors that result from the determination of Young's modulus, as well as the contact area, are mainly due on the one hand to the accuracy/precision of the measured forces distribution and on the other hand to the estimation of the contact between the probe (cantilever) and the cell. In the first case, the measurement accuracy of the force distribution has been discussed in the previous sections. By combining dynamic and static approaches for the spring cantilever calibration, the overall sensitivity of the optical detection device has been enhanced. In the second case, the morphology of cells (which depends on the cell life evolution) induces local modification on the contact mechanics between the probe and the cell. Furthermore, common models that predict the elastic deformation of soft materials are restricted to spherical-shape materials. As the size of the cell is involved in the Hertz, DMT, and JKR analytical models, the change on cell morphology can affect the mechanical cell property determination.

In the following, we propose to conduct an analytical study to evaluate the uncertainties depending on these two cases. First, uncertainties due to measurements can easily be estimated. Regarding the deformation, which is dependent on the applied load, errors can be attributed to the acquisition system, starting with the measurement of the engines' displacement. Uncertainties on these displacements are already estimated at 3%. Both the calibration of the stiffness of the cantilever, which are seen below, and the measurement of the spot deviation are used to obtain load data. The estimated error for the measurement of the spot deviation is 0.5%. The last uncertainty regards the location of the cell on the cantilever and the equivalent contact point. They were evaluated [23], and the global uncertainties on the measurement of load and strain are about 8%. This value, which was calculated in the worst case, can be reduced to 5% for an expert on the FBM.

The second error source in the assessment of Young's modulus comes from the contact between the cell and the cantilever. The modeling of this contact needs knowledge of the cell's radius. Its determination, without prejudicial contact, is based on the visual estimation of the cell surface under the microscope. The ratio between the surface and the radius were preliminarily determined on several tests on cells. Moreover, for adhesion models, adhesion energy estimation is realized by the measurement of pull-off forces. The great variability of these forces implies the assessment of its influence on Young's modulus.

To identify the comportment of our model regarding these two parameters, the crushing simulation of a perfect and homogeneous sphere is used. This first study investigates the influence of the error made on Young's modulus related to the cell's radius uncertainty. The plot of the stress as a function of the strain of the spheres with an increasing radius (2, 4, 6, 8, and 10 $\mu$m) submitted to a known load [0–0.5 $\mu$N] is realized for the three models (Fig. 15). Several conclusions regarding Young's modulus (represented by the slope of these curves) can be drawn. The steep slopes with a small strain, for the DMT model, represent the stiffness effect by adhesion and do not correspond to the cell stiffness. The JKR model is the one where slopes are the most steady during all load tests. Moreover, the influence of the radius is really soft for this model and negligible for strains such as $\epsilon > 0.05$. The JKR model, which is, by definition, appropriate for cellular studies, is also less sensitive to errors in the determination of the cell's radius.

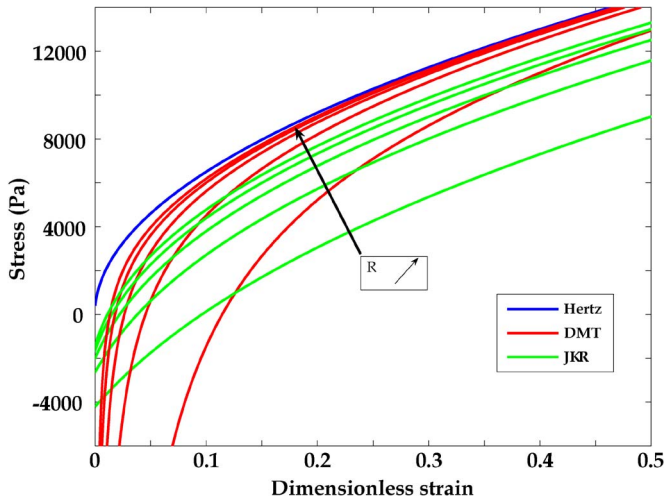


Fig. 15. Stress versus strain for indentation of a perfect sphere with different radius.

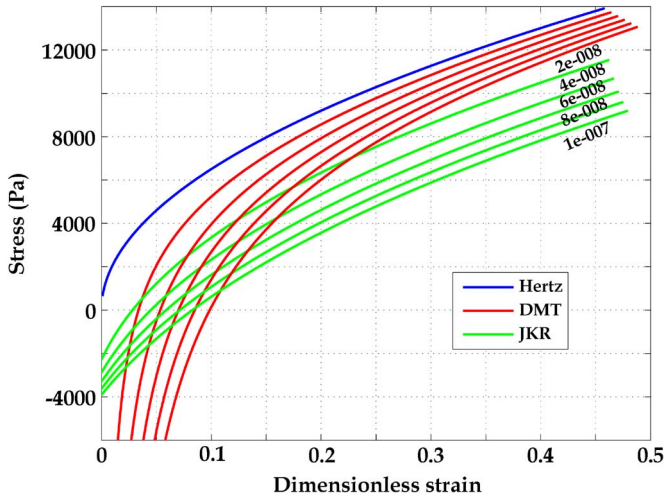


Fig. 16. Stress versus strain for indentation of a perfect sphere with different pull-off forces.

The indentation of a sphere (radius 5 $\mu$m) is then realized for variable pull-off forces [20, 40, 60, 80, 100 nN]. For each model, the stress-versus-strain curves are plotted in Fig. 16. In the same way, we notice that the DMT model strongly diverges for small strains. The assessment of Young's modulus for $\epsilon < 0.2$ should lead to great errors. On the contrary, the JKR model is steady for all the elongations investigated and show a small deviation for $\epsilon > 0.05$.

The JKR model for soft solids with high adhesion energy (as cell does) is slightly sensitive to both radius variations and pull off forces, which are the two uncertain parameters for this modeling. Young's modulus is estimated for $\epsilon > 0.05$, with a cumulative error of 5% on the model. Nevertheless, given the large diversity and the great complexity of cells, studies will lead to as many cells as possible.

## VI. Conclusion

This paper has presented the development of a microforce sensing system for *in vitro* mechanotransduction investigation. The experimental setup combines SPM techniques with advanced robotics approaches. As the developed system operates in a fully automatic mode based on visual and force tracking control, effective mechanical characterization and reliable data acquisition are achieved. The FBM device consists of three modules with autonomous force sensing and measurement capabilities. Each module is designed, calibrated, or configured toward an effective and reliable device.

Experiments have been conducted using the FBM on human adherent cervix *EpH* cells. The experiments demonstrate the efficiency of the experimental setup developed to explore the mechanical response in *in vitro* conditions of adherent biological samples. The contact mechanisms that result from the cell mechanical characterization process are predicted using appropriate models, taking into account both adhesion forces and finite sample thickness.

## References


[1] M. Girot, M. Boukallel, and S. Régnier, "An hybrid micro-force sensing device for mechanical cell characterization," in *Proc. Int. Conf. Instrum. Meas. Technol.*, Sorrento, Italy, Apr. 2006, pp. 501–506.

[2] Y. Sun and B.-J. Nelson, "Microrobotic cell injection," in *Proc. Int. Conf. Robot. Autom.*, Seoul, Korea, May 2001, pp. 620–625.

[3] K. J. Van Vliet, G. Bao, and S. Suresh, "The biomechanics toolbox: Experimental approaches for living cells and biomolecules," *Acta Mater.*, vol. 51, no. 19, pp. 5881–5905, Nov. 2003.

[4] D.-H. Kim, S. Yun, and B. Kim, "Mechanical force response of single living cells using a microrobotic system," in *Proc. Int. Conf. Robot. Autom.*, New Orleans, LA, Apr. 2004, pp. 5013–5018.

[5] J. Guck, R. Ananthakrishnan, C.-C. Cunningham, and J. Kas, "Stretching biological cells with light," *J. Phys. Condens. Matter*, vol. 14, no. 19, pp. 4843–4856, May 2002.

[6] J. M. Sharp, A. R. Clapp, and R. B. Dickinson, "Measurement of long-range forces on a single yeast cell using a gradient optical trap and evanescent wave light scattering," *Colloids Surf., B Biointerfaces*, vol. 27, no. 4, pp. 355–364, Mar. 2003.

[7] M. Lukkari and P. Kallio, "Multi-purpose impedance-based measurement system to automate microinjection of adherent cells," in *Proc. Int. Symp. Comput. Intell. Robot. Autom.*, 2005, pp. 20–26.

[8] M. Radmacher, "Measuring the elastic properties of biological samples with the AFM," *IEEE Eng. Med. Biol. Mag.*, vol. 16, no. 2, pp. 47–57, Mar./Apr. 1997.

[9] O. Sahin, G. Yaralioglu, R. Grow, S. F. Zappe, A. Atalar, C. Quate, and O. Solgaard, "High-resolution imaging of elastic properties using harmonic cantilevers," *Sens. Actuators, A, Phys.*, vol. 114, no. 2/3, pp. 183–190, Sep. 2004.

[10] S. Park, K. Costa, and G. Ateshian, "Microscale frictional response of bovine articular cartilage from atomic force microscopy," *J. Biomech.*, vol. 37, no. 11, pp. 1679–1687, Nov. 2004.

[11] Y. Sun and B.-J. Nelson, "MEMS for cellular force measurements and molecular detection," *J. Inf. Acquis.*, vol. 1, no. 1, pp. 23–32, Jan. 2004.

[12] E. K. Dimitriadis, F. Horkay, J. Maresca, B. Kachar, and R. S. Chadwick, "Determination of elastic moduli of thin layers of soft material using the atomic force microscope," *Biophys. J.*, vol. 82, no. 5, pp. 2798–2810, May 2002.

[13] X. Yao, J. Walter, S. Burke, S. Stewart, M. H. Jericho, D. Pink, R. Hunter, and T. J. Beveridge, "Atomic force microscopy and theoretical considerations of surface properties and turgor pressures of bacteria," *Colloids Surf., B Biointerfaces*, vol. 23, no. 2/3, pp. 213–230, Feb. 2002.

[14] R. E. Mahaffy, C. K. Shih, F. C. Mackintosh, and J. Kas, "Scanning probe-based frequency-dependent microrheology of polymer gels and biological cell," *Phys. Rev. Lett.*, vol. 85, no. 4, pp. 880–883, Jul. 2000.

[15] M. Kim, J. Choi, and Y. Park, "Calibration of the spring constants of various AFM cantilevers with the small uncertainty level of 2%," in *Proc. Int. Joint Conf. SICE-ICASE*, Oct. 2006, pp. 2532–2537.

[16] J. E. Sader, "Method for the calibration of atomic force microscope cantilever," *Rev. Sci. Instrum.*, vol. 66, no. 7, pp. 3789–3798, Jul. 1995.

[17] R. Levy and M. Maaloum, "Measuring the spring constant of atomic force microscope cantilevers: Thermal fluctuations and other methods," *Nanotechnol.*, vol. 13, no. 1, pp. 33–37, Feb. 2002.

[18] K. L. Johnson and J. A. Greenwood, "An adhesion map for the contact of elastic spheres," *J. Colloid Interface Sci.*, vol. 92, no. 2, pp. 326–333, Aug. 1997.

[19] J. Domke and M. Radmacher, "Measuring the elastic properties of thin polymer films with the atomic force microscope," *Langmuir*, vol. 14, no. 12, pp. 3320–3325, May 1998.

[20] B. B. Akhremitchev and G. C. Walker, "Finite sample thickness effects on elasticity determination using atomic force microscopy," *Langmuir*, vol. 15, no. 17, pp. 5630–5634, Jun. 1999.

[21] K. D. Costa and F. C. Yin, "Analysis of indentation: Implications for measuring mechanical properties with atomic force microscopy," *Trans. ASME, J. Biomech. Eng.*, vol. 121, no. 5, pp. 462–471, Oct. 1999.

[22] D. Maugis, *Contact, Adhesion and Rupture of Elastic Solids*. Berlin, Germany: Springer-Verlag, 2000.

[23] M. Girot, "Force-bio-microscope for cells mechanotransduction studies," Ph.D. dissertation, Univ. Pierre et Marie Curie, Paris, France, Jul. 2007.


**Maxime Girot** received the Ph.D. degree in mechanics and robotics from the University Pierre et Marie Curie, Paris, France, in 2007.

He has been an Associate Professor of classes préparatoires aux grandes écoles with the Institut des Systèmes Intelligents et Robotique, Université Pierre et Marie Curie, Paris, since 2007. His research interests are focused on mechanotransduction and biological characterization.

**Mehdi Boukallel** received the M.S. degree in automation and micromechanics and the Ph.D. degree in robotics, automation, and computer science from the Université de Franche-Comté, Besancon, France, in 2000 and 2003, respectively.

From 2003 to 2004, he was a Research Staff Member with the Microrobotics Group, Besançon. From 2005 to 2007, he was a Postdoctoral Researcher of micromanipulation and nanomanipulation with the Université Pierre et Marie Curie, Paris, France. He is currently a Senior Researcher with the Microrobotics Group, Commissariat à l'Energie Atomique, Paris. His research interests include microrobotics design, biomanipulation, scanning probe microscopy, and control of smart actuators.

**Stéphane Régnier** received the Ph.D. degree in mechanics and robotics from the University Pierre et Marie Curie, Paris, France, in 1996.

He is currently an Associate Professor with the Institut des Systèmes Intelligents et Robotique, Université Pierre et Marie Curie, Paris, where he has been the Head of the Micromanipulation Team since 2001. His research interests are focused on micromanipulation and nanomanipulation, teleoperation and haptic feedback at the nanoscale, micromechatronics, and biological cell characterization.